ACS Catalysis

Research Article

pubs.acs.org/acscatalysis

NH_3 Decomposition for H_2 Generation: Effects of Cheap Metals and Supports on Plasma–Catalyst Synergy

Li Wang,[†] Yanhui Yi,[†] Yue Zhao,[†] Rui Zhang,[†] Jialiang Zhang,[‡] and Hongchen Guo*[,†]

[†]State Key Laboratory of Fine Chemicals, Department of Catalytic Chemistry and Engineering, Dalian University of Technology (DUT), Dalian 116024, P. R. China

[‡]School of Physics and Optoelectronic Engineering, DUT, Dalian 116024, P. R. China

Supporting Information

ABSTRACT: NH_3 decomposition is important because of its potential use in generating CO-free H_2. In this study, several cheap metals (Fe, Co, Ni, and Cu) and a series of supports (zeolite materials: TS-1 um, TS-1 nm, HZSM-5 nm, and NaZSM-5 nm; SiO_2-based materials: fumed SiO_2 and SiO_2-ball; and metal oxide materials: r′-Al_2O_3 and TiO_2) were used to prepare supported catalysts. X-ray fluorescence, N_2 physisorption, X-ray diffraction, transmission electron microscopy, Fourier-transform infrared spectroscopy, temperature-programmed desorption, mass spectrometry, temperature-programmed reduction, and electrical property analysis were used to investigate the effect of the catalyst on the synergy between a plasma (produced by dielectric barrier discharge) and the catalyst in NH_3 decomposition. The results show that the synergy depends strongly on the strength of the metal–nitrogen (M–N) bond, and the relative dielectric constant (ε_d) of the support. When Fe, Co, Ni, and Cu were supported on fumed SiO_2, the order of the strengths of the M–N bonds was Cu–N < Ni–N < Co–N < Fe–N. Among the catalysts, Co/fumed SiO_2 showed a stronger synergy with the plasma and gave higher NH_3 conversion in plasma catalysis. Co catalysts supported on fumed SiO_2, SiO_2-ball, and r′-Al_2O_3, which have small ε_d values, had stronger synergies with plasma and therefore gave higher NH_3 conversions. The relative dielectric constant of the support correlated well with NH_3 conversion in plasma catalysis. These results show that the relative dielectric constant is an essential parameter in developing catalyst supports for plasma conditions. This study provides direct proof that the recombinative desorption of adsorbed N atoms is the rate-limiting step in the catalytic decomposition of NH_3 over cheap metal catalysts such as Fe, Co, and Ni and that there is synergy between plasma and cheap metal catalysts in plasma-catalytic NH_3 decomposition.

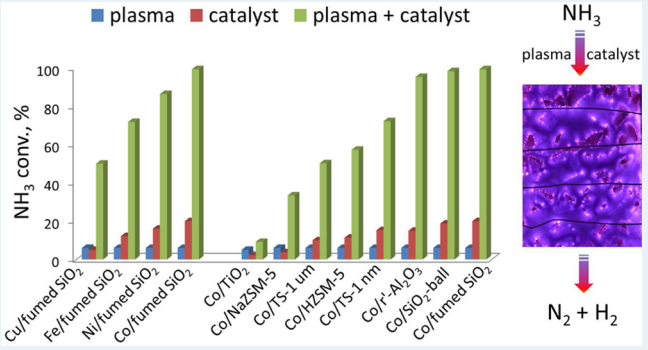

KEYWORDS: *hydrogen energy, ammonia decomposition, plasma catalysis, synergy, cheap metal, relative dielectric constant of support*

1. INTRODUCTION

In recent years, NH_3 decomposition has received considerable attention because of its potential use in CO-free H_2 production for fuel cell devices.[1−4] Traditional heterogeneous catalysis has so far been the main route for NH_3 decomposition.[5−10] Although noble-metal Ru catalysts perform well, the scarcity of such catalysts limits their use.[11−19] The main problem with cheap metals (such as Fe and Ni) is the slow recombinative desorption rate of adsorbed N atoms (N_{ad}) from active sites, which makes them less active in NH_3 decomposition, unless the reaction is conducted at high temperatures (>500 °C).[2,8,20,21] To solve this problem, the use of various promoters,[22−24] bimetallic catalysts,[25−29] supports,[8,17−19] transition metal nitrides and carbides,[30−32] and catalyst preparation methods[33−35] have been studied. However, much effort is still needed to develop cheap metal catalysts for NH_3 decomposition under mild temperatures.

Recently, we proposed an efficient method, i.e., dielectric barrier discharge (DBD) plasma catalysis, for NH_3 decomposition. For example, when a commercially available bulk Fe-based catalyst[36] was used for NH_3 decomposition, NH_3 conversion increased from 7.4% to 99.9% after placing the bulk Fe-based catalyst in a plasma zone at 410 °C. This shows that unexpected synergy occurred between the plasma and bulk Fe-based catalyst. We have demonstrated that a plasma can accelerate the recombinative desorption rate of N_{ad} from a bulk Fe-based catalyst; this is one of the main factors of synergy.[37] This plasma catalysis route also has advantages such as high catalyst heating rate and high energy efficiency in H_2 production compared with traditional heterogeneous catalysts. These advantages are attributed to internal heating via gas discharge. A high catalyst heating rate results in a quick response to in situ H_2 generation from NH_3, e.g., in cold starting cars. The device for DBD plasma catalysis is simple and

Received: November 30, 2014
Revised: May 28, 2015
Published: May 29, 2015

DOI: 10.1021/acscatal.5b00728
ACS Catal. 2015, 5, 4167−4174

consists mainly of a small transformer and a small reactor. The reactor can be regarded as a fixed-bed reactor with two electrodes. This simplicity is useful in practical applications.

In this study, the effects of cheap metals and their supports on synergy in plasma-catalytic NH_3 decomposition were systematically investigated as part of our ongoing efforts to understand the synergy between plasma and cheap metals. We believe that our studies will broaden the scope of heterogeneous catalysis.

2. EXPERIMENTAL SECTION

2.1. DBD Plasma-Catalytic Reactor. NH_3 decomposition was performed in a DBD reactor, with a catalyst bed in the discharge zone, at atmospheric pressure (Scheme S1). The reactor had two coaxial bare-metal electrodes. The shell was a quartz tube (10 mm o.d. × 8 mm i.d.) and also served as the dielectric barrier. The outer ground electrode was Al foil (0.1-mm-thick) wrapped tightly around the surface of the quartz tube. The inner high-voltage electrode was a stainless-steel rod (2 mm o.d.; surface composition: Fe 68.5 wt %. Cr 19.9 wt %, Ni 8.1 wt %, Mn 2.0 wt %, Si 0.5 wt %,Cu 0.7 wt %, Ag 0.1 wt %, Al 0.1 wt %, and C 0.1 wt %); it was installed along the axis of the quartz tube. An alternating current (AC) supply was used,[38] and a catalyst was embedded in the plasma zone. Before discharge, an NH_3 feed (99.999% purity) was flowed through the reactor for 30 min to remove air, and then the DBD plasma was generated by switching on the AC power supply. NH_3 was decomposed to N_2 and H_2 by the DBD plasma and the catalyst. The products were analyzed using an online gas chromatograph equipped with a thermal conductivity detector for N_2 and NH_3 detection. The total power in the plasma-catalytic NH_3 decomposition was measured using a power meter (MASTECH MS2203, Hong Kong). The AC supply power was determined from the product of the apparent voltage and current of the AC supply, and the input power of the plasma reactor was measured using a digital oscilloscope (Tektronix DPO 3012 digital oscilloscope equipped with a Tektronix P6015A high-voltage probe and a Pearson 6585 current probe, USA), as shown in Scheme S2 and Figure S1.

The rate of H_2 formation ($mol \cdot g^{-1} \cdot h^{-1}$), defined as the number of moles of H_2 produced per gram of catalyst per hour, was calculated using eq 1. The energy efficiency of H_2 formation [$mol \cdot g^{-1}(kW \cdot h)^{-1}$] defined as the number of moles of H_2 produced per gram of catalyst per kilowatt hour, was calculated using eq 2. The synergistic capability (Q) was defined as the conversion of NH_3 in the case of plasma + catalyst, minus the sum of NH_3 conversions in the cases of plasma alone and catalyst alone; Q was calculated using eq 3.

$$R_{H_2} = \frac{3 \cdot X_{NH_3} \cdot F_{NH_3} \times 60}{2 \times 1000 \times 22.4 \cdot m_c} \quad (1)$$

$$E_{H_2} = \frac{3 \cdot X_{NH_3} \cdot F_{NH_3} \times 60}{2 \times 1000 \times 22.4 \cdot m_c \cdot P} \quad (2)$$

where R_{H_2} is the rate of H_2 formation in $mol \cdot g^{-1} \cdot h^{-1}$, E_{H_2} is the energy efficiency of H_2 formation in $mol \cdot g^{-1}(kW \cdot h)^{-1}$, X_{NH_3} is the NH_3 conversion, F_{NH_3} is the NH_3 flow rate in $mL \cdot min^{-1}$, m_c is the catalyst mass in g, and P is the plasma power in kW.

$$Q = X_{NH_3(p-c)} - (X_{NH_3(p)} + X_{NH_3(c)}) \quad (3)$$

where Q is the synergistic capability, $X_{NH_3(p-c)}$ is the NH_3 conversion with plasma + catalyst, $X_{NH_3(p)}$ is the NH_3 conversion with plasma, and $X_{NH_3(c)}$ is the NH_3 conversion with catalyst.

2.2. Catalyst Preparation. Metal (Fe, Co, Ni, and Cu) nitrates were provided by the Tianjin Kermel Chemical Reagent Co., Ltd., China. The zeolite supports (TS-1 um, TS-1 nm, NaZSM-5 nm, and HZSM-5 nm) were synthesized using a hydrothermal method. The properties of the supports are shown in Figure S2 and Table S1. Other supports (TiO_2, r′-Al_2O_3, fumed SiO_2, and SiO_2-ball) were purchased from the Dalian Luming Nanometer Material Co., Ltd., China. All the catalysts were prepared using an incipient wet impregnation method. Briefly, the metal nitrate (30 wt % metal in the final catalyst) was dissolved in deionized water. The support was calcined at 400 °C for 5 h to remove impurities such as H_2O before impregnation, and then the pretreated support was added to the metal nitrate solution. The mixture was kept at room temperature for 3 h, vacuum freeze-dried overnight at −50 °C, and dried in the air at 120 °C for 5 h. Dried samples were calcined in a He-DBD plasma environment at 540 °C for 3 h.

2.3. Characterization of Support and Catalyst. The support acidity was evaluated by NH_3 temperature-programmed desorption (NH_3-TPD; Quantacchrome ChemBET 3000 chemisorption instrument, USA). The sample (140 mg) was pretreated at 600 °C for 1 h in a He flow (20 $mL \cdot min^{-1}$) and then cooled to 150 °C. The pretreated sample was saturated with NH_3 for 30 min and then purged with a He flow for 1 h at 150 °C. The TPD profile was recorded while the sample was heated from 150 to 600 °C at a constant heating rate of 14 $°C \cdot min^{-1}$ in a He flow.

N_2 physisorption was performed at −196 °C (Micrometrics ASAP 2020 instrument, USA).[39] Prior to the N_2 physisorption measurements, the samples were degassed at 350 °C for 3 h. The specific surface areas (S_g) of the samples were calculated using the Brunauer−Emmett−Teller (BET) equation.

The electrical capacity (C_d) of the support material was measured at 12 kHz (Fluke PM6304, Fluke, 0.0 pF to 100 mF, USA), and the relative dielectric constant (ε_d) was calculated using eq 4.

$$C_d = \frac{S_d \varepsilon_0 \varepsilon_d}{l_d} \quad (4)$$

where ε_d is the relative dielectric constant of support, ε_o is the dielectric constant in a vacuum, ≈ $8.854187817 \times 10^{-12}$ $F \cdot m^{-1}$, C_d is the electrical capacity of support in pF, S_d is the support area in m^2, and l_d is the support thickness in m.

The metal chemical states and particle sizes of catalysts were determined using X-ray diffraction (XRD; Rigaku D-Max 2400, Cu K_a radiation, Japan) and transmission electron microcopy (TEM; FEI Tecnai F30 microscope, point resolution 0.20 nm, operated at 300 kV, Holland), respectively. The metal loading on the supported catalyst was determined using X-ray fluorescence (XRF; SRS-3400, Bruker, Germany). The adsorption of NH_3 molecules on the catalyst surface was studied using Fourier transform infrared spectroscopy (FTIR; Nicolet 6700 spectrometer equipped with a liquid-N_2-cooled mercy cadmium telluride detector, USA). Metal−support interactions were studied using temperature-programmed reduction (TPR; Quantacchrome ChemBET 3000, USA). The metal−nitrogen (M−N) bond strengths were investigated

DOI: 10.1021/acscatal.5b00728
ACS Catal. 2015, 5, 4167−4174

using a TPD system coupled with an online mass spectrometer (MS; OmniStar GSD 301, USA).

3. RESULTS

3.1. Synergy between Plasma and Cheap Metal Catalysts in NH_3 Decomposition. The NH_3 conversion increased significantly when a plasma was combined with the catalyst, regardless of which metal (Figure 1) or support

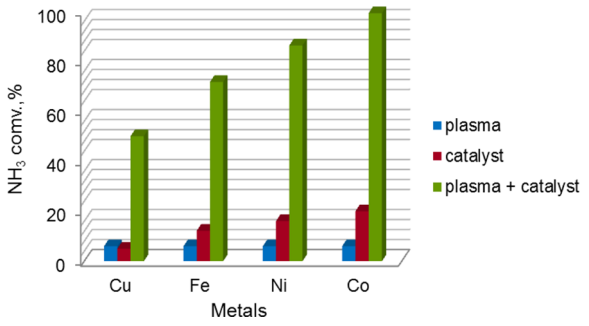

Figure 1. Influence of metals on NH_3 conversion in plasma + catalyst, plasma, and catalyst modes. (Fumed SiO_2 support, NH_3 feed rate 40 mL·min^{-1}, temperature 450 °C, supported catalyst 0.88 g, discharge gap 3 mm, discharge frequency 12 kHz; in the catalyst case, the temperature was provided by an electric heating furnace; In the plasma and plasma + catalyst cases, the temperature originated from the electric heat released by the plasma, and was determined using an IR camera and thermocouple tightly attached to the outer wall of the reactor, as shown in Scheme S3 and Figure S3; AC supply power is shown in Table S2.)

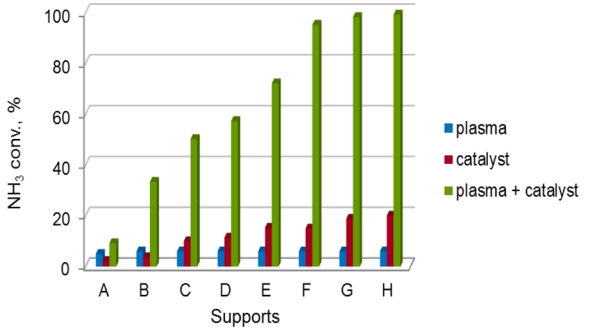

Figure 2. Influence of supports on NH_3 conversion in plasma + catalyst, plasma, and catalyst modes: (A) TiO_2, (B) NaZSM-5 nm, (C) TS-1 um, (D) HZSM-5 nm, (E) TS-1 nm, (F) r′-Al_2O_3, (G) SiO_2-ball, (H) fumed SiO_2. (Active component Co, NH_3 feed rate 40 mL·min^{-1}, temperature 450 °C, supported catalyst 0.88 g, discharge gap 3 mm, discharge frequency 12 kHz; AC supply power is shown in Table S3.)

(Figure 2) was used. The NH_3 conversion achieved using plasma + catalyst mode was much higher than the sum of those obtained using a plasma and a catalyst alone. For example, over the Co/fumed SiO_2 catalyst, the plasma + catalyst mode gave an NH_3 conversion of 99.2%, whereas the sum of the NH_3 conversions using a plasma and a catalyst alone was only 26.0%. The rate of H_2 formation, calculated using eq 1, was higher for plasma + catalyst than for a catalyst alone (Tables S2 and S3). These results show clear synergy between the plasma and the catalysts. This synergy strongly depends on the types of metals and supports. The data in Table 1 show that in the plasma + catalyst mode, the synergistic capability (Q) of the catalyst

Table 1. Synergistic Capabilities (Q) of Plasma with Various Catalysts[a]

catalyst	synergistic capability (Q)	catalyst	synergistic capability (Q)
Co/fumed SiO_2 (H)	73%	Fe/fumed SiO_2	54%
Co/r′-Al_2O_3 (G)	74%	Co/fumed SiO_2	73%
Co/SiO_2-ball (F)	73%	Ni/fumed SiO_2	64%
Co/TS-1 nm (E)	51%	Cu/fumed SiO_2	39%
Co/HZSM-5 nm (D)	40%		
Co/TS-1 um (C)	34%		
Co/NaZSM-5 nm (B)	24%		
Co/TiO_2 (A)	2%		

[a]Q was calculated by eq 3.

decreased in the order of Co > Ni > Fe > Cu when fumed SiO_2 was used as the support, and in the order of fumed SiO_2 ≈ r′-Al_2O_3 ≈ SiO_2-ball > TS-1 nm > HZSM-5 nm > TS-1 um > NaZSM-5 nm > TiO_2 when Co metal was used as the catalyst.

3.2. Characterizations. The physicochemical properties of the supports, the chemical states and dispersion of metals, the metal−support interactions, and the reactant adsorption and product desorption on the catalysts were determined using various techniques, to investigate the plasma−catalyst synergy and the effects of the metals and supports on the synergy.

3.2.1. Physicochemical Properties of Supports. The XRD patterns (Figure S4) shows that the zeolite supports (TS-1 um, TS-1 nm, HZSM-5 nm, and NaZSM-5 nm) and the metal oxide supports (r′-Al_2O_3 and TiO_2) are the crystalline materials, whereas the SiO_2-based supports (fumed SiO_2 and SiO_2-ball) are amorphous materials. The NH_3-TPD profiles (Figure S5) show large differences among the acidities of the supports. The data in Table 2 show that the supports also have different

Table 2. Physicochemical Properties of Supports Used in This Study

supports	phase state	specific surface area (S_g, m^2·g^{-1})[a]	average pore size (nm)	electric capacity (C_d, pF)	relative dielectric constant (ε_d)[b]
fumed SiO_2	amorphous	297.79		27.77	19.99
SiO_2-ball	amorphous	194.79	7.97	28.56	20.56
TS-1 nm	crystal	397.37	0.55	28.72	20.68
r′-Al_2O_3	crystal	111.66	6.97	29.20	21.02
TS-1um	crystal	365.57	0.54	29.87	21.51
HZSM-5	crystal	265.09	0.55	31.75	22.86
NaZSM-5	crystal	273.08	0.54	33.33	24.00
TiO_2	crystal (anatase)	14.22		36.91	26.58

[a]Specific surface area (S_g) is calculated by the BET equation. [b]Relative dielectric constant was calculated by eq 4.

specific surface areas (S_g) and average pore sizes and electrical properties. The electrical capacity (C_d) values of the supports are in the range of 27.77−36.91 pF, and the corresponding relative dielectric constants (ε_d) are in the range of 19.99−26.58.

DOI: 10.1021/acscatal.5b00728
ACS Catal. 2015, 5, 4167−4174

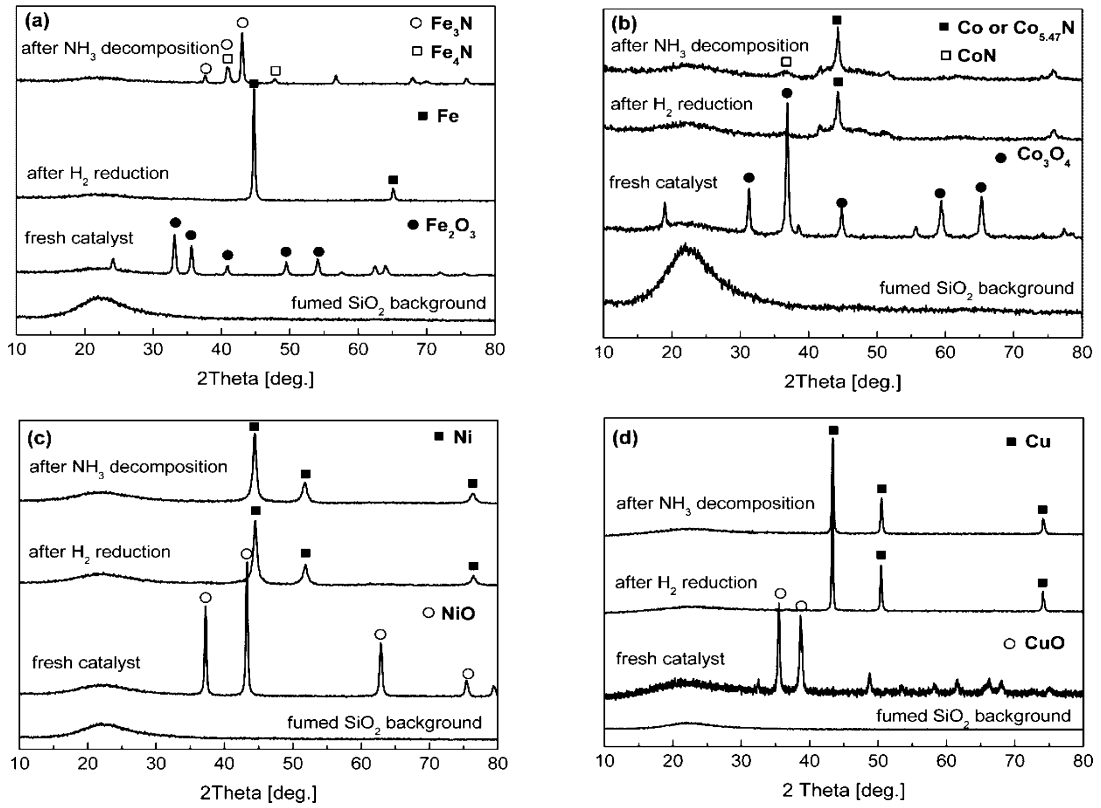

Figure 3. XRD patterns of various metal catalysts supported on fumed SiO_2: (a) Fe, (b) Co, (c) Ni, and (d) Cu. (Fe_2O_3, ICCD: 33−664; Fe, ICCD: 6-696; Fe_3N, ICCD: 1-1236; Fe_4N, ICCD: 6-627; Co_3O_4, ICCD: 42−1467; Co, ICCD: 15-806; NiO, ICCD: 22-1189; Ni, ICCD: 4-850; CuO, ICCD: 41−254; Cu, ICCD: 4-836.)

3.2.2. Chemical States of Supported Metals. The XRD patterns (Figure 3) show that the supported Fe, Co, Ni, and Cu all underwent similar chemical state changes during reduction in the H_2 plasma and plasma-catalytic NH_3 decomposition, regardless of the support used. For example, when supported by fumed SiO_2, the as-prepared Fe, Co, Ni, and Cu existed as oxides (Fe_2O_3, Co_3O_4, NiO, and CuO). They were transformed to the metallic states (Fe, Co, Ni, and Cu) after reduction in H_2 plasma. However, significant differences were observed when the metallic catalysts were used for plasma-catalytic NH_3 decomposition; i.e., during plasma-catalytic NH_3 decomposition, the Ni and Cu catalysts remain in their metallic states. However, the Co catalyst was partly transformed to the nitride. The Fe catalyst was completely nitrided to form Fe_3N and Fe_4N.

3.2.3. Metal Dispersion of Catalysts. TEM images of various metals supported on fumed SiO_2 and Co supported on various supports are shown in Figures 4 and 5, respectively. Figure 4 shows that the average sizes of the Fe, Co, Ni, and Cu particles on the fumed SiO_2 support were about 5, 3, 3−8, and 5 nm, respectively, indicating high dispersion of the metals. Figure 5 shows that, except in the case of NaZSM-5, highly dispersed Co particles were formed on all the supports, namely fumed SiO_2, SiO_2-ball, TiO_2, r′-Al_2O_3, TS-1 nm, TS-1 um, and HZSM-5 nm. The average Co particle size was less than 5 nm, mostly around 2−3 nm. In the case of NaZSM-5, the average Co particle size was about 50 nm. It is inferred that the higher aggregation of Co particles on NaZSM-5 than on HZSM-5 is caused by sodium ions.

3.2.4. Metal−Support Interactions. H_2-TPR was used to investigate the metal−support interactions. Figure 6 shows that

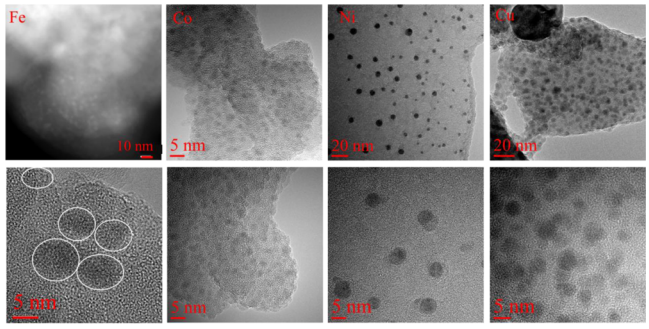

Figure 4. TEM images of Fe, Co, Ni, and Cu catalysts supported on fumed SiO_2 (reduced in H_2 plasma).

the reduction of Co_3O_4 on various supports mainly occurs in the temperature range 300−550 °C. The reduction temperatures increase in the order fumed SiO_2 < SiO_2-ball < r′-Al_2O_3 < TS-1 nm < HZSM-5 nm < TS-1 um < NaZSM-5 nm < TiO_2, which means that the interactions between Co and these supports increase in the same order. It is worth noting that on most supports Co_3O_4 shows two reduction peaks. Literature reports[40−42] suggest that the lower-temperature peak can be attributed to the reduction of Co_3O_4 to CoO, and the higher-temperature peak can be assigned to the reduction of CoO to metallic Co. In the case of the r′-Al_2O_3 support, a third reduction peak appears in a much higher temperature region, from 600 to 750 °C. It has been suggested that this peak can be assigned to Co^{x+} ions incorporated into the crystal lattice of the support.[42,43] Such Co^{x+} ions have the strongest interactions with the support.

DOI: 10.1021/acscatal.5b00728
ACS Catal. 2015, 5, 4167−4174

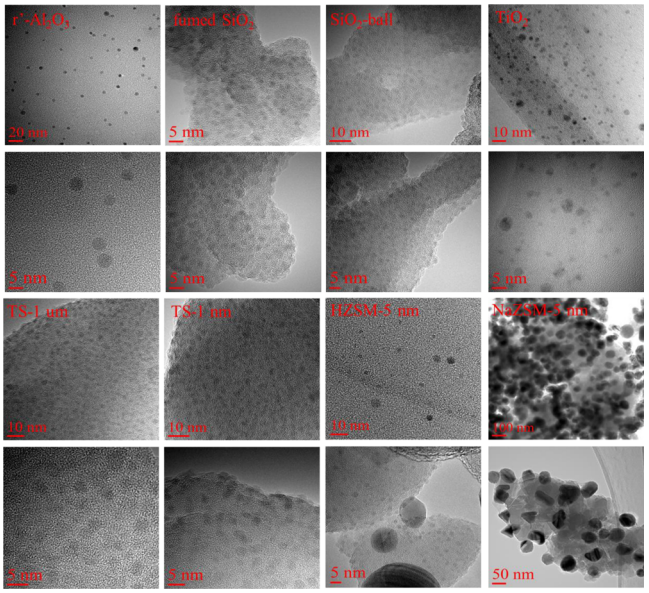

Figure 5. TEM images of Co on various supports (reduced in H_2 plasma).

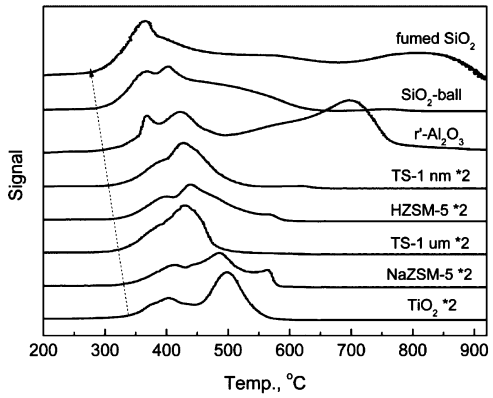

Figure 6. TPR profiles of Co catalysts on various supports. (Catalysts used in the TPR experiment were as-prepared fresh catalysts, see Figure 3b. "*" represents that attenuation coefficient of the signal.)

3.2.5. Adsorption of Reactant on Supported Metal Catalysts. The adsorption of NH_3 on the Fe, Co, Ni, and Cu catalysts was studied using FTIR (Figure 7). The results show that there were abundant adsorbed NH_2 ($NH_{2,ad}$) species on the catalyst surfaces, but no NH_{ad} species were detected. The amount of $NH_{2,ad}$ varied depending on the metals. When the adsorption temperature was increased from 350 to 450 °C, the $NH_{2,ad}$ species on the Cu catalyst disappeared, but the amount of such species on the Fe catalyst was almost unchanged. These results indicate that dissociative adsorption of NH_3 occurred on these catalysts. Different metals have different bonding abilities toward $NH_{2,ad}$ species: the Cu−$NH_{2,ad}$ bond is weakest, and the Fe−$NH_{2,ad}$ bond is the strongest.

3.2.6. Desorption of Products from Supported Metal Catalysts. In online mass spectrometry (MS) during NH_3 decomposition on the supported Fe, Co, and Ni catalysts alone, an intense H_2 signal was detected almost immediately after the injection of NH_3 (Figure 8). However, only a weak N_2 signal

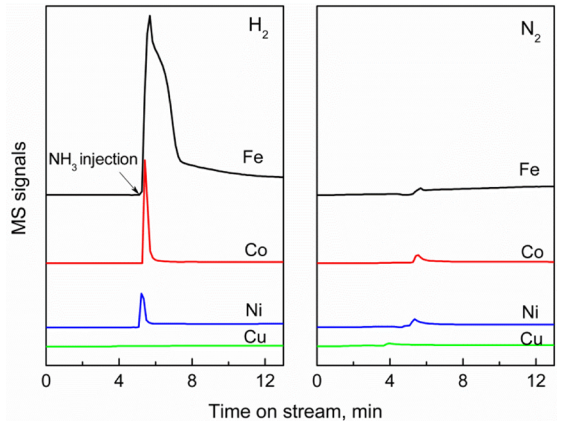

Figure 8. Online MS analysis of the initial stage of NH_3 decomposition over Fe, Co, Ni, and Cu catalysts supported on fumed SiO_2 without plasma (0.95 g of metal catalyst was prepared in a H_2 flow for 3 h at 500 °C and cooled to 450 °C in a He flow to remove H_2; the flow was switched to 40 mL·min^{-1} NH_3 for reaction at 450 °C).

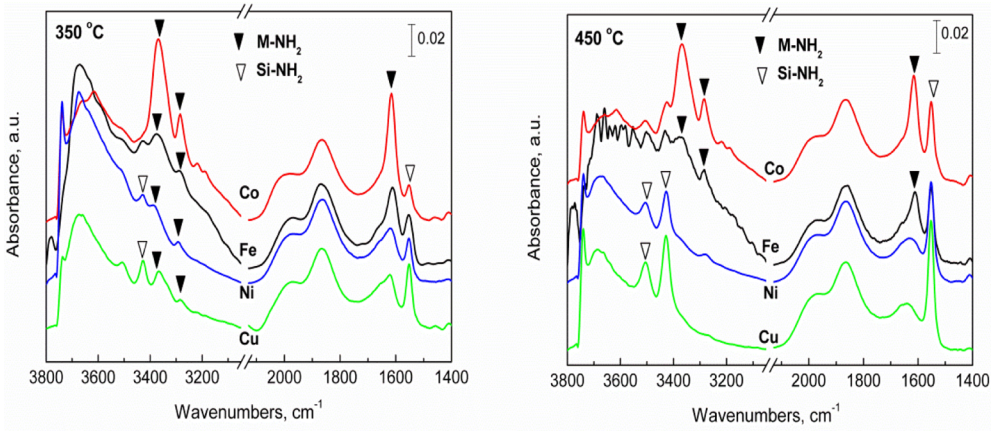

Figure 7. IR spectra for NH_3 adsorption on Fe, Co, Ni, and Cu catalysts supported on fumed SiO_2. (Samples were treated by in situ H_2 reduction at 500 °C; NH_3 adsorption was conducted at 350 and 450 °C, respectively, followed by outgassing at 200 °C. IR bands at 3365, 3280, and 1610 cm^{-1} are attributed to asymmetric stretching, symmetric stretching, and asymmetric deformation, respectively, of NH_2 amide species adsorbed on metal sites.[44] The band at 1440 cm^{-1} is tentatively assigned to imido NH deformation.[45])

DOI: 10.1021/acscatal.5b00728
ACS Catal. 2015, 5, 4167−4174

was observed for these catalysts. The H_2 signal attenuated sharply with time and then leveled off. These results show that H_2 desorption is easy, but N_2 desorption from these metals is difficult, in the absence of a plasma. The majority of N atoms are absorbed on the Fe, Co, and Ni catalyst surface by forming strong M−N bonds. The H_2 and N_2 signals for the Cu catalyst were much weaker than those for the Fe, Co, and Ni catalysts; this is attributed to low NH_3 decomposition activity of the Cu catalyst.

The relative M−N bond strengths (M = Fe, Co, Ni, and Cu) were investigated using TPD. Figure 9 shows that considerable

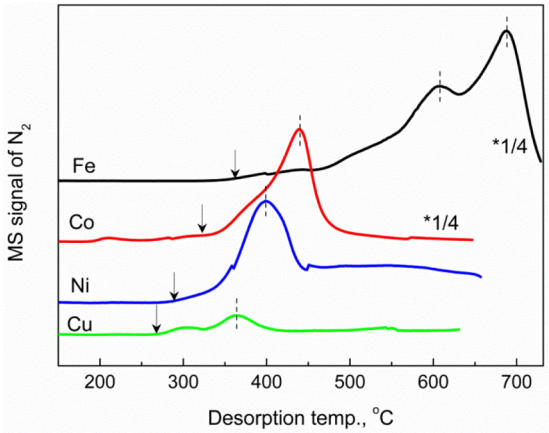

Figure 9. TPD profiles of supported Fe, Co, Ni, and Cu catalysts obtained from the same experiment as in Figure 8. (After reaction, these catalysts were cooled in situ to room temperature in a NH_3 flow.)

amounts of N_2 were released from the Fe, Co, and Ni catalysts; this is why only small amounts of N_2 were detected by MS and the H_2 signal intensities decreased with time during NH_3 decomposition over these catalysts in the absence of a plasma (Figure 8). A comparison of the profiles shows that the temperature needed for N_2 desorption increases significantly from Cu to Ni, Co, and Fe. These results show that the strength of the M−N bond increases from Cu to Ni, Co, and Fe; i.e., the Fe−N bond is the strongest, and the Cu−N bond is the weakest.

4. DISCUSSION

4.1. Comparison of Metals. The metal dispersion has an important effect on the catalytic activity of a supported metal catalyst. In a comparative study, we observed that for a similar Co loading of about 28 wt %, the NH_3 conversion on a Co/fumed SiO_2 catalyst with a Co particle of size 3 nm was much higher than that of a Co/fumed SiO_2 catalyst with a Co particle of size >20 nm in the catalyst and plasma + catalyst (Figures S6 and S7). In this study, for similar particle sizes and metal loadings (Figure 4 and Table S4), we mainly focused on the differences among metals in plasma-catalytic NH_3 decomposition. Figure 8 shows that fresh metallic Fe, Co, Ni, and Cu catalysts show different initial H_2 productivities (Fe > Co > Ni > Cu); this shows that metallic Fe, Co, Ni, and Cu have different abilities to dissociate the N−H bond of NH_3. The N−H bond dissociation abilities of these metals (metallic state) decreases in the order Fe > Co > Ni > Cu. The sharp decreases in H_2 productivity and postreaction studies of the catalysts (Figures 9 and 3) show that the fresh metallic Fe, Co, and Ni catalysts were nitrided in the initial stage of NH_3 decomposition. The Fe and Co catalysts were substantially transformed into nitrides during this process (Figure 3), while the Ni catalyst was probably transformed into surface nitride. However, compared with their metallic counterparts, the nitrided Fe, Co, and Ni catalysts all showed lower catalytic activities. These results are consistent with those reported in the literature.[46] These observations were used to compare the synergies of different catalysts (Figures 1 and 2) based on the postnitridation catalysts, which are steady catalysts. Figures 8 and 9 also provide direct experimental proof that the recombinative desorption of bonded N atoms from the cheap metal catalysts (Fe, Co, and Ni) is the rate-limiting step in catalytic NH_3 decomposition. Currently, direct empirical evidence is still lacking in the literature.[12,22]

The M−N bond strength is one of the key factors in NH_3 decomposition over cheap metal catalysts; metals with moderate M−N bond strengths (Co−N) show higher activities (Figures 1 and 9). If the M−N bond is too weak, dissociative adsorption of NH_3 on the metal is difficult and desorption of the $NH_{2,ad}$ intermediate species before further dehydrogenation is easy, resulting in low catalytic activity. This was the case for the supported Cu catalysts (Figure 7). Boisen et al. reported that the activity of Cu in catalytic NH_3 decomposition is lower than those of other metal catalysts.[9] However, if the M−N bond is too strong, dissociative adsorption of NH_3 on the metal will occur easily, but desorption of the bonded N atoms from the catalyst will be difficult; therefore highly active metal sites are difficult to recover. This was the case for the supported Fe catalysts (Figures 8 and 9). The reason for the different synergies of Fe, Co, Ni, and Cu catalysts with a plasma, shown in Figure 1, can be mainly attributed to their different M−N bond strengths.

It should be pointed out that although Co has a moderate M−N bond strength, NH_3 decomposition over the Co catalyst alone gave very low conversion (~20%), as shown in Figure 1. The recombinative desorption of the bonded N atoms is still the rate-limiting step. However, when NH_3 decomposition was performed in plasma + Co catalyst mode, NH_3 conversion reached almost 100%. The role of the plasma in this synergy is to accelerate the recombinative desorption of bonded N atoms.[37] Clearly, this acceleration effect of the plasma works not only in the case of Co catalysts but also for Fe and Ni catalysts. Figure 10 gives more direct proof that the role of the plasma in the plasma−catalyst synergy can be attributed to acceleration of the rate-limiting step of NH_3 decomposition, i.e., the recombinative desorption of bonded N atoms from the Fe, Co, and Ni catalysts. In the case of the supported Cu catalysts, significant plasma−catalyst synergy is also observed. The recombinative desorption of bonded N atoms is not a problem for Cu catalysts; therefore other types of synergy between the plasma and Cu catalyst may be involved. This is a subject for future research.

4.2. Comparison of Supports. As mentioned above (Figure 2), the support has a significant effect on the plasma−catalyst synergy in NH_3 decomposition. The effect of the support on the synergy was investigated using a series of supported Co catalysts with similar Co loadings and particle sizes (Table S4 and Figure 5). A comparison of the results for the reactions and characterizations of the catalysts showed that the specific surface area, average pore size, phase state (crystalline or amorphous), and acidity of the support (Table 2 and Figure S5) had no obvious effects on the synergy. The

DOI: 10.1021/acscatal.5b00728
ACS Catal. 2015, 5, 4167−4174

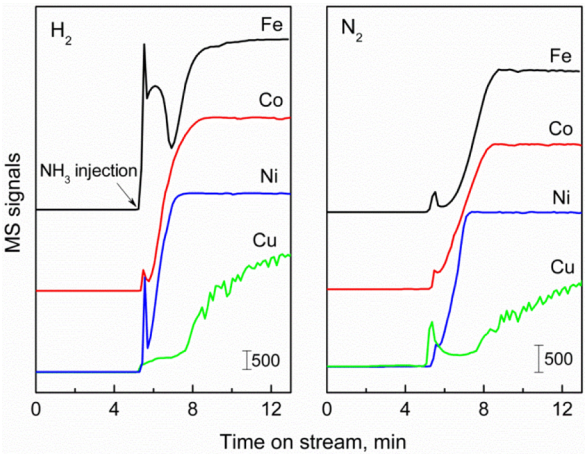

Figure 10. Online MS analysis of initial stage of NH_3 decomposition over Fe, Co, Ni, and Cu catalysts in plasma + catalyst mode. (Fumed SiO_2 was used as the support; 0.95 g of metal catalyst was prepared in H_2 flow for 3 h at 500 °C, followed by cooling to 250 °C in He flow to remove H_2, and then switching to 40 mL·min^{-1} NH_3 flow for reaction under an AC supply power of about 28 W, and the final temperature was kept stable at around 450 °C.)

effect of support on the synergy is closely related to the metal−support interactions and the electrical properties of the support.

Figure 6 shows that the order of the strengths of the interactions of Co with various supports is fumed SiO_2 < SiO_2-ball < r′-Al_2O_3 < TS-1 nm < HZSM-5 nm < TS-1 um < NaZSM-5 nm < TiO_2. This order is consistent with that for NH_3 decomposition (Figure 2). Clearly, weak interactions favor NH_3 decomposition.

Figure 11 shows that the relative dielectric constant (ε_d) of the support also correlates well with plasma-catalytic NH_3

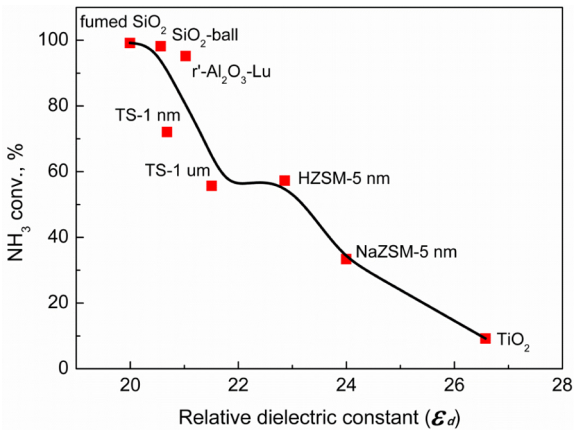

Figure 11. NH_3 conversions on Co catalysts on various supports as a function of relative dielectric constants of supports in plasma + catalyst mode. (NH_3 feed 40 mL·min^{-1}, temperature 450 °C, supported catalyst 0.88 g, discharge gap 3 mm, discharge frequency 12 kHz.)

decomposition. The decomposition decreases significantly with increasing ε_d. A support with a small ε_d facilitates plasma-catalytic NH_3 decomposition. To understand the influence of the relative dielectric constant of the support, NH_3 decomposition was performed in plasma + bare support mode (Figure 12). It can be seen that on replacement of the catalysts with the bare supports, NH_3 decomposition decreases significantly with increasing ε_d of the support. We took NH_3

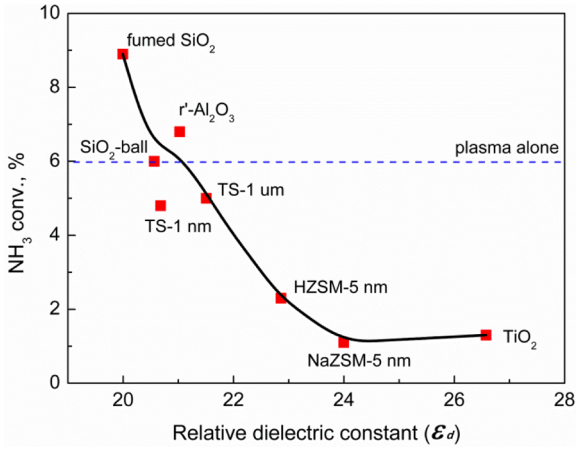

Figure 12. NH_3 conversions on different supports as a function of relative dielectric constants of supports in plasma + bare support mode. (NH_3 feed 40 mL·min^{-1}, temperature 450 °C, bare support 0.88 g, discharge gap 3 mm, discharge frequency 12 kHz.)

conversion in plasma mode as a reference (NH_3 conversion was 6%, shown by a dashed line) and found that fumed SiO_2, r′-Al_2O_3, and SiO_2-ball have weak but positive effects on NH_3 conversion, whereas other supports such as HZSM-5, NaZSM-5, and TiO_2 have negative effects on NH_3 conversion.

The support plays an important role in traditional heterogeneous catalysis; this is generally related to the specific surface area, porosity, acidity, and support−metal strong interactions. However, the electrical properties of support are seldom mentioned in traditional heterogeneous catalysis. In the area of plasma catalysis, a few researchers have attempted to promote reactions by filling the plasma zone with high-dielectric-constant materials.[47,48] To the best of our knowledge, materials with different dielectric constants have not been studied as catalyst supports, at least in the area of plasma catalysis. The similarity in the sequences of ε_d−NH_3 conversion relationships in Figures 11 and 12 shows that the relationship can be attributed to the influence of the support on the high-voltage discharge that produced the plasma. In the plasma zone, the net electric field decreases because of accumulation of electrons on the solid surface, especially for supports with large ε_d values.

5. CONCLUSION

This study provides direct proof that recombinative desorption of adsorbed N atoms is the rate-limiting step in the catalytic decomposition of NH_3 over cheap metal catalysts, and that a synergy exists between a plasma and cheap metal catalysts. The synergy strongly depends on the M−N bond strengths and, in particular, on the relative dielectric constant of the support in plasma-catalytic NH_3 decomposition. The order of M−N bond strengths is Cu−N < Ni−N < Co−N < Fe−N, when Fe, Co, Ni, and Cu are supported on fumed SiO_2. Metals such as Co that form M−N bonds of moderate strength are expected to enhance the plasma−catalyst synergy and therefore give higher NH_3 conversions in plasma catalysis. Supports with small ε_d values, i.e., fumed SiO_2, SiO_2-ball, and r′-Al_2O_3, give stronger synergies and higher NH_3 conversions. This indicates that the relative dielectric constant is an essential parameter in developing supports for catalysts used under plasma conditions.

DOI: 10.1021/acscatal.5b00728
ACS Catal. 2015, 5, 4167−4174

■ ASSOCIATED CONTENT

Supporting Information

The Supporting Information is available free of charge on the ACS Publications website at DOI: 10.1021/acscatal.5b00728.

Experimental setup of plasma-catalytic NH_3 decomposition; measurement of temperature and plasma power; XRD, NH_3-TPD, SEM, specific surface areas, and pore volumes of supports; energy efficiency and rates of H_2 formation; influence of metal particle size on the activity of NH_3 decomposition; metal loading of supported catalysts (PDF)

■ AUTHOR INFORMATION

Corresponding Author

*Tel./fax: +86-411-84986120. E-mail: hongchenguo@163.com.

Notes

The authors declare no competing financial interest.

■ ACKNOWLEDGMENTS

We acknowledge financial support from the Natural Science Foundation of China (NSFC, 20473016 and 20673018) and the State Key Laboratory of Fine Chemicals of Dalian University of Technology.

■ REFERENCES

(1) García-Bordejé, E.; Armenise, S.; Roldán, L. *Catal. Rev.: Sci. Eng.* **2014**, *56*, 220−237.
(2) Schüth, F.; Palkovits, R.; Schlögl, R.; Su, D. S. *Energy Environ. Sci.* **2012**, *5*, 6278−6289.
(3) Lan, R.; Irvine, J. T. S.; Tao, S. W. *Int. J. Hydrogen Energy* **2012**, *37*, 1482−1494.
(4) Klerke, A.; Christensen, C. H.; Nørskov, J. K.; Vegge, T. *J. Mater. Chem.* **2008**, *18*, 2304−2310.
(5) Tagliazucca, V.; Schlichte, K.; Schüth, F.; Weidenthaler, C. *J. Catal.* **2013**, *305*, 277−289.
(6) Li, X. K.; Ji, W. J.; Zhao, J.; Wang, S. J.; Au, C. T. *J. Catal.* **2005**, *236*, 181−189.
(7) Yin, S. F.; Xu, B. Q.; Zhou, X. P.; Au, C. T. *Appl. Catal., A* **2004**, *277*, 1−9.
(8) Yin, S. F.; Zhang, Q. H.; Xu, B. Q.; Zhu, W. X.; Ng, C. F.; Au, C. T. *J. Catal.* **2004**, *224*, 384−396.
(9) Boisen, A.; Dahl, S.; Nørskov, J. K.; Christensen, C. H. *J. Catal.* **2005**, *230*, 309−312.
(10) Obata, K.; Kishishita, K.; Okemoto, A.; Taniya, K.; Ichihashi, Y.; Nishiyama, S. *Appl. Catal., B* **2014**, *160−161*, 200−203.
(11) Karim, A. M.; Prasad, V.; Mpourmpakis, G.; Lonergan, W. W.; Frenkel, A. I.; Chen, J. G.; Vlachos, D. G. *J. Am. Chem. Soc.* **2009**, *131*, 12230−12239.
(12) Hansgen, D. A.; Vlachos, D. G.; Chen, J. G. *Nat. Chem.* **2010**, *2*, 484−489.
(13) Huang, D. C.; Jiang, C. H.; Liu, F. J.; Cheng, Y. C.; Chen, Y. C.; Hsueh, K. L. *Int. J. Hydrogen Energy* **2013**, *38*, 3233−3240.
(14) Li, Y. X.; Yao, L. H.; Song, Y. Y.; Liu, S. Q.; Zhao, J.; Ji, W. J.; Au, C. T. *Chem. Commun.* **2010**, *46*, 5298−5300.
(15) Raróg-Pilecka, W.; Szmigiel, D.; Kowalczyk, Z.; Jodzis, S.; Zielinski, J. *J. Catal.* **2003**, *218*, 465−469.
(16) García-García, F. R.; Guerrero-Ruiz, A.; Rodríguez-Ramos, I. *Top. Catal.* **2009**, *52*, 758−764.
(17) Li, L.; Wang, Y. H.; Xu, Z. P.; Zhu, Z. H. *Appl. Catal., A* **2013**, *467*, 246−252.
(18) Marco, Y.; Roldán, L.; Armenise, S.; García-Bordejé, E. *ChemCatChem* **2013**, *5*, 3829−3834.
(19) Li, G.; Nagasawa, H.; Kanezashi, M.; Yoshioka, T.; Tsuru, T. *J. Mater. Chem. A* **2014**, *2*, 9185−9192.
(20) Liu, H. C.; Wang, H.; Shen, J. H.; Sun, Y. Z.; Liu, M. *Appl. Catal., A* **2008**, *337*, 138−147.
(21) Donald, J.; Xu, C. B.; Hashimoto, H.; Byambajav, E.; Ohtsuka, Y. *Appl. Catal., A* **2010**, *375*, 124−133.
(22) Zheng, W. Q.; Zhang, J.; Ge, Q. J.; Xu, H. Y.; Li, W. Z. *Appl. Catal., B* **2008**, *80*, 98−105.
(23) Liu, H. C.; Wang, H.; Shen, J. H.; Sun, Y.; Liu, Z. M. *Catal. Today* **2008**, *131*, 444−449.
(24) Li, Y. X.; Yao, L. H.; Liu, S. Q.; Zhao, J.; Ji, W. J.; Au, C. T. *Catal. Today* **2011**, *160*, 79−86.
(25) Lorenzut, B.; Montini, T.; Bevilacqua, M.; Fornasiero, P. *Appl. Catal., B* **2012**, *125*, 409−417.
(26) Simonsena, S. B.; Chakraborty, D.; Chorkendorff, I.; Dahl, S. *Appl. Catal., A* **2012**, *447−448*, 22−31.
(27) Duan, X. Z.; Qian, G.; Zhou, X. Q.; Chen, D.; Yuan, W. K. *Chem. Eng. J.* **2012**, *207−208*, 103−108.
(28) Zhang, J.; Müller, J.; Zheng, W. Q.; Wang, D.; Su, D. S.; Schlögl, R. *Nano Lett.* **2008**, *8*, 2738−2743.
(29) Hansgen, D. A.; Thomanek, L. M.; Chen, J. G.; Vlachos, D. G. *J. Chem. Phys.* **2011**, *134*, 184701−184707.
(30) Zheng, W. Q.; Cotter, T. P.; Kaghazchi, P.; Jacob, T.; Frank, B.; Schlichte, K.; Zhang, W.; Su, D. S.; Schüth, F.; Schlögl, R. *J. Am. Chem. Soc.* **2013**, *135*, 3458−3464.
(31) Soerijanto, H.; Rödel, C.; Wild, U.; Lerch, M.; Schomäcker, R.; Schlögl, R.; Ressler, T. *J. Catal.* **2007**, *250*, 19−24.
(32) Otremba, T.; Frenzel, N.; Lerch, M.; Ressler, T.; Schomäker, R. *Appl. Catal., A* **2011**, *392*, 103−110.
(33) Yao, L. H.; Li, Y. X.; Zhao, J.; Ji, W. J.; Au, C. T. *Catal. Today* **2010**, *158*, 401−408.
(34) Lu, A. H.; Nitz, J. J.; Comotti, M.; Weidenthaler, C.; Schlichte, K.; Lehmann, C. W.; Terasaki, O.; Schüth, F. *J. Am. Chem. Soc.* **2010**, *132*, 14152−14162.
(35) Duan, X. Z.; Qian, G.; Zhou, X. G.; Sui, Z. J.; Chen, D.; Yuan, W. K. *Appl. Catal., B* **2011**, *101*, 189−196.
(36) Liu, H. Z. *Chin. J. Catal.* **2014**, *35*, 1619−1640.
(37) Wang, L.; Zhao, Y.; Liu, C. Y.; Gong, W. M.; Guo, H. C. *Chem. Commun.* **2013**, *49*, 3787−3789.
(38) Zhang, J.; Li, T.; Wang, D. J.; Zhang, J. L.; Guo, H. C. *Chin. J. Catal.* **2015**, *36*, 274−282.
(39) Zheng, B. M.; Wan, Y. F.; Yang, W. H.; Ling, F. X.; Xie, H.; Fang, X. C.; Guo, H. C. *Chin. J. Catal.* **2014**, *35*, 1800−1810.
(40) Jongsomjit, B.; Panpranot, J.; Goodwin, J. G. *J. Catal.* **2001**, *204*, 98−109.
(41) Tang, C. W.; Wang, C. B.; Chien, S. H. *Thermochim. Acta* **2008**, *473*, 68−73.
(42) Fischer, N.; Minnermann, M.; Baeumer, M.; van Steen, E.; Claeys, M. *Catal. Lett.* **2012**, *142*, 830−837.
(43) Arnoldy, P.; Moulijn, J. A. *J. Catal.* **1985**, *93*, 38−54.
(44) Wang, L.; Xin, Q.; Zhao, Y.; Zhang, G.; Dong, J.; Gong, W. M.; Guo, H. C. *ChemCatChem* **2012**, *4*, 624−627.
(45) Ramis, G.; Yi, L.; Busca, G.; Turco, M.; Kotur, E.; Willey, R. J. *J. Catal.* **1995**, *157*, 523−535.
(46) Pelka, R.; Kiełbasa, K.; Arabczyk, W. *J. Phys. Chem. C* **2014**, *118*, 6178−6185.
(47) Rico, V. J.; Hueso, J. L.; Cotrino, J.; Gallardo, V.; Sarmiento, B.; Brey, J. J.; González-Elipe, A. R. *Chem. Commun.* **2009**, 6192−6194.
(48) Pan, K. L.; Chung, W. C.; Chang, M. B. *IEEE Trans. Plasma Sci.* **2014**, *42*, 3809−3818.

DOI: 10.1021/acscatal.5b00728
ACS Catal. 2015, 5, 4167−4174